

STATIC AND DYNAMIC BEHAVIOR OF WATER DROPLETS ON THE HETEROGENEOUS PLATINUM SURFACE

Tae Woo Kwon^a, Matthew Stanley Ambrosia^b and Man Yeong Ha^{a*}

^a School of Mechanical Engineering, Pusan National University, San 30, Jangjeon-dong, Geumjeong-gu, Busan 609-735, Korea

^b Department of Environmental Administration, Catholic University of Pusan, 57 Oryundae-ro, Geumjeong-gu, Busan 609-757, Korea

E-mail: megaktw@naver.com

ABSTRACT

In this study, the static and dynamic behaviors of water droplets on heterogeneous surfaces were investigated using molecular dynamics simulations. The surface consisted of the flat plate and pillar structures. The pillar was designed with two heights and three characteristic energies. The simulations were conducted in two steps. In the first step, the water droplet reached the static equilibrium state as a sphere or hemisphere. The static behaviors of the water droplets were in the Wenzel or the Cassie-Baxter state. In the next step, the five forces applied to the water droplets. The dynamic behaviors of the water droplets could be classified into three groups. And the effects of the pillar characteristic energy and the magnitude of the applied force on the behaviors were discussed using the contact angle hysteresis. It was found that a weak pillar characteristic energy had a larger effect on the short pillar height while a stronger pillar characteristic energy had a greater effect on the high pillar height.

INTRODUCTION

The ability of a solid surface to repel water is called hydrophobicity. This characteristic is very important in areas such as self-cleaning materials and fluid flow over a surface. Static hydrophobicity can be controlled by characteristic energy and surface roughness and can be evaluated by two different theories proposed by Wenzel [1] and Cassie and Baxter [2]. Water fills up the gaps between the structures in the Wenzel state. Conversely, in the Cassie-Baxter state, the water sits on top of the structures.

However, not all droplets on rough surfaces can be grouped in only the Wenzel state or Cassie-Baxter state. Marmur [3] shows conditions between the Wenzel and Cassie-Baxter states where a part of the water droplet permeates the space between the structures. Milne [4] describes some examples in which the Cassie equation cannot predict the contact angle. In this study, however, the structure of the surface consists of square pillars and a flat plate which result in either the Wenzel or the Cassie-Baxter state in almost all cases.

NOMENCLATURE

Symbols

C	[-]	Value to control the force
E	[kcal/mol]	Pillar characteristic energy
F	[kcal/mol]	Body force
G	[Å]	Gap size between pillars
H	[Å]	Pillar height
L	[Å]	Length of the surface
P	[Å]	Lateral size of the pillar
r_{ij}	[Å]	Distance between a pair of atoms
R_{\min}	[Å]	van der Waals radius
$R_{\min,s}$	[Å]	Solid plate characteristic length
U		Potential
x		Cartesian axis direction
y		Cartesian axis direction
z		Cartesian axis direction

Greek symbols

ε	[kcal/mol]	Characteristic energy
ρ	[-]	Density
θ	[°]	Contact angle

Sub/superscripts

Ad	Advanced position
p	Pillar
Re	Receding position
s	Surface
x	Cartesian axis direction
y	Cartesian axis direction
z	Cartesian axis direction

Mathematical symbols

$\langle \rangle$	Surface-averaged value
-------------------	------------------------

It is more difficult to control of dynamic hydrophobicity in comparison to that of static hydrophobicity due to the movement of the water droplet. Several studies have been conducted to evaluate dynamic hydrophobicity [5-16]. While static contact angles have an effect on dynamic hydrophobicity, the contact angle hysteresis has been used to evaluate dynamic hydrophobicity which is related to the difference between the advancing and receding contact angles [5-12].

There are many theoretical and experimental studies related to the dynamic hydrophobicity of water droplets on surfaces which gives information helpful to understand phenomena at the macroscopic scale [1-21]. However, there are few studies on dynamic hydrophobicity of water droplets at the nano-scale using molecular dynamics (MD) simulations [22-25].

In this paper, the static and dynamic behaviors of a water droplet on heterogeneous surfaces were investigated using MD simulations. The heterogeneous surfaces consist of a flat plate and nano-sized pillar structures with three different characteristic energies. This means that the substance of the plate and pillars are different. The behavior of water droplets on the heterogeneous surfaces are evaluated and compared with those on the homogeneous surfaces which have a plate and pillars of the same characteristic energy.

NUMERICAL METHODOLOGY

The NAMD simulation package is used to simulate the static and dynamic behaviors of a water droplet on the heterogeneous surfaces. NAMD was developed by the Theoretical and Computational Biophysics Group (TCB) and the Parallel Programming Laboratory (PPL) at the University of Illinois in Urbana-Champaign [26].

MD simulations model the physical movement of atoms by calculating the sum of the different forces on those atoms and solving Newton's equations of motion. To calculate those forces, the potentials are used. The functional form is

$$U_{total} = U_{bonded} + U_{non-bonded} \quad (1)$$

The first term on the right hand side, U_{bonded} describes the sum of the bonded potential energies such as the atomic bond potential, the angle potential and the dihedral potential. The second term on the right hand side, $U_{non-bonded}$ is non-bonded potentials included the Lennard-Jones and electrostatic potentials. The Lennard-Jones potential, U_{LJ} explains the van der Waals forces attracting and repelling other atoms between the two atoms.

$$U_{LJ} = 4\epsilon_{ij} \left[\left(\frac{R_{min}}{r_{ij}} \right)^{12} - \left(\frac{R_{min}}{r_{ij}} \right)^6 \right] \quad (2)$$

where ϵ_{ij} and R_{min} are the characteristic energy and van der Waals radius, respectively. The distance between a pair of atoms is represented by r_{ij} .

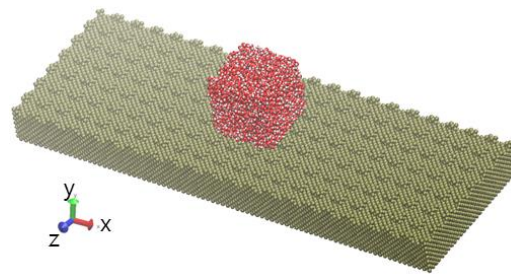


Figure 1 Coordinate system, computational domain, and initial shape of water cube

Figure 1 shows the coordinate system, computational domain, and initial shape of water cube used in present study. The number of water molecules was 3921. The water molecules were initially placed in the shape of a cube on a rectangular surface whose size was $L_x \times L_z = 356.16 \text{ \AA} \times 118.72 \text{ \AA}$. The structure of the surfaces were (100) platinum which has a face centered cubic structure. The location of the surface atoms were fixed in the static and dynamic simulations.

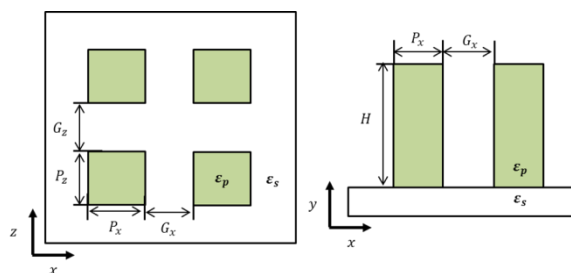


Figure 2 Schematic view of the shape of pillars and their arrangement on the pillar-patterned surface

Figure 2 shows the shape of the pillars and their arrangement on the surface. The lateral size of the pillars, $P_x \times P_z$, was fixed at $8.48 \text{ \AA} \times 8.48 \text{ \AA}$ on the basis of the distance of the center of the atoms. The gap size, $G_x \times G_z$, was equal to the lateral size. The height of the pillars varied from 4.24 \AA to 16.96 \AA .

We focused on the behavior of water droplets by varying the water-solid interaction energy of the pillars while keeping the characteristic energy of the plate constant. The characteristic energy of the pillars varied: $\epsilon_p = 0.1, 0.3$ and 0.5 kcal/mol. The characteristic energy of the plate, ϵ_s , however, was fixed at 0.3 kcal/mol.

The NVT ensemble was used, which keeps the number of atoms, volume, and temperature constant as the calculations proceeded. The temperature was set to 298.15 K and controlled using the velocity scaling method [26]. The periodic boundary condition was applied with a domain size of $356.16 \text{ \AA} \times 255.00 \text{ \AA} \times 118.72 \text{ \AA}$ in x, y and z directions, respectively. The x and z dimensions matched the surface and the y dimension was chosen to be large enough to ensure that interactions beyond the domain in the y -direction were insignificant.

The TIP3P water model was used to set the water molecules. The TIP3P water model has three charges, -0.834 kcal/mol for

the O atom and +0.417 kcal/mol for the H atoms arranged in a triangle with an angle of 104.52°. The length of the bond is 0.9572 Å between the O and H atoms. Evaporation was insignificant and neglected in these simulations. The long-range charge-charge interactions between the water molecules were calculated by using the Ewald method. Newton's equation of motion was integrated numerically using the velocity Verlet algorithm with a time step of 2.0 fs.

The simulation was conducted in two steps. In the first step, the objective was for the water molecules to reach an equilibrium state from an initial cube. In a water droplet, molecules are always moving and changing positions so the contact angle changes continually. However, if the contact angle which is averaged over time is constant, the state is considered an equilibrium state. In this study, 5 ns was chosen as the time to reach an equilibrium state because the averaged contact angle was stable over the time. The aim in the second step was to evaluate the dynamic behavior of the water droplet sliding on heterogeneous surfaces and compare the results to those of a homogeneous surface. As shown in Figure 3, we applied constant body forces to the water droplets obtained from the first step in the x -direction for an additional 5 ns. The body force applied to the water droplet in the x -direction was defined as $F = \exp(C\varepsilon_s / R_{\min,s})$, where ε_s and $R_{\min,s}$ represents the solid characteristic energy and the solid plate characteristic length, respectively. Three different C values were used to apply three different forces to the water droplets, as shown in Table 1.

Table 1 Constant body forces applied

C $F = \exp(C\varepsilon_s / R_{\min,s})$	Force	
	kcal/mol	nN/mol
10	0.1353	5.6628
20	0.0183	0.7664
30	0.0025	0.1037

To measure the hydrophobicity of the pillared surface for the different cases considered in this study, the intrinsic contact angles of the water droplets on the surfaces were computed first. The following computational approach was used to determine the water droplet shapes and contact angles. From the computational results for the trajectory of all of the water molecules, the x -, y - and z -coordinates of all the water molecules were obtained. The density $\bar{\rho}$ of the water droplet was defined as the average number of water molecules in a given unit cubic cell with a side length of 3Å. To make the density field smooth, the density was calculated using a smoothed distribution $\hat{\rho}$ obtained from $\bar{\rho}$ though several successive applications of a spatially weighted average over the surrounding grid points. In three dimensions, the elementary smoothing procedure around a given grid point (i, j, k) is expressed as follows by expanding the 3-dimensional smoothing procedures given by Bonometti *et al.*

$$\hat{\rho}_{i,j,k} = \frac{3}{4}\bar{\rho}_{i,j,k} + \frac{1}{24}(\bar{\rho}_{i-1,j,k} + \bar{\rho}_{i+1,j,k} + \bar{\rho}_{i,j-1,k} + \bar{\rho}_{i,j+1,k} + \bar{\rho}_{i,j,k-1} + \bar{\rho}_{i,j,k+1}) \quad (3)$$

The density field was normalized in order that its highest value was scaled to be one. To extract the water droplet contact angle from the density field, the water droplet periphery was defined as the circular line with a density value $\hat{\rho}$ of 0.5 using a least-squares fitting through the water droplet periphery [26]. The contact angle was defined as the angle between a tangential line of the droplet periphery where it contacts the surface and a line from the droplet periphery where it contacts the surface to the droplet's projected center of mass on the top surface of the pillars.

A subscript notation was used for simplicity and readability. The pillar characteristic energy, the pillar height, and the applied force are represented by E , H , and F , respectively. Table 2 defines these values according to its subscript.

Table 2 Subscript notation for the pillar characteristic energy, the pillar height and the force applied to the water droplet

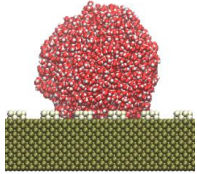
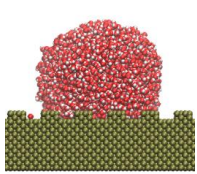
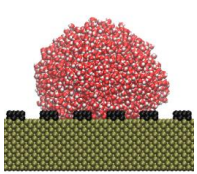
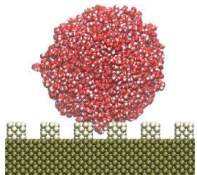
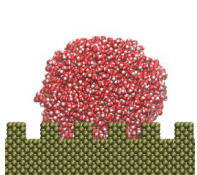
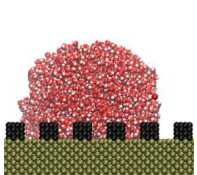
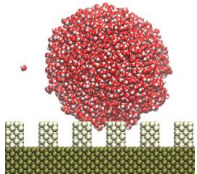
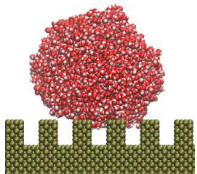
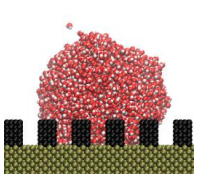
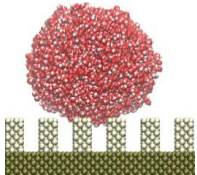
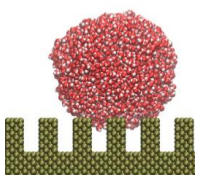
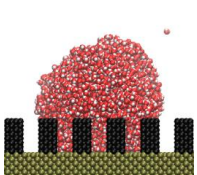
Subscript	Pillar Characteristic Energy (E)	Pillar Height (H)	Force (F)
1	0.1 kcal/mol	4.24 Å	$C=30$
2	0.3 kcal/mol	8.48 Å	$C=20$
3	0.5 kcal/mol	12.72 Å	$C=10$
4	-	16.96 Å	

RESULTS OF STATIC STATE

To evaluate the results of the dynamic state more effectively, it is essential to know the equilibrium state of the water droplets on their respective surfaces before the force is applied. The contact angle of the static state is calculated every 5 ps. And the values are time-averaged over 2ns.

Table 3 shows schematics, static state and contact angles for different values of pillar height H and the pillar characteristic energy ε_p . Here H is the dimensionless pillar height which is defined as the pillar height divided by 4.24 Å and ε_p is the characteristic energy of the pillar. The static state and contact angle in equilibrium state are related to the characteristics of the pillar. When the height of the pillar increases, the contact angle increases and the state of the water droplet changes from the Wenzel state to the Cassie-Baxter state. Particularly, in the case of the homogeneous surface whose characteristic energy of the pillar is 0.3 kcal/mol in the second column, the Cassie-Baxter state appears at the 12.72 Å height of the pillar with 25% surface fraction. These results are similar to those of the study by Ambrosia *et al* [29]. The characteristic energy of the pillar also affects the contact angles. When the characteristic energy of the pillar is weak in the first column, the Cassie-Baxter state appears at the 8.48 Å pillar height. However, for the strong characteristic energy of the pillar the Wenzel state can be seen at all pillar heights. This shows that the strong characteristic energy of the pillar can lead to decrease the hydrophobicity of the surface for the same geometry.

Table 3 Schematics, static state and contact angles for different values of pillar height H and the pillar characteristic energy ε_p

Pillar Height (H)	Static state & contact angle								
	$\varepsilon_p = 0.1kcal / mol$		$\varepsilon_p = 0.3kcal / mol$		$\varepsilon_p = 0.5kcal / mol$				
	Figure		Figure		Figure				
	State	Angle [°]	State	Angle [°]	State	Angle [°]			
1		Wenzel	126.42		Wenzel	121.32		Wenzel	115.29
2		Cassie	143.97		Wenzel	122.15		Wenzel	111.51
3		Cassie	142.56		Cassie	137.06		Wenzel	111.85
4		Cassie	143.62		Cassie	136.47		Wenzel	107.13

RESULTS OF DYNAMIC STATE

In this study, the effect of heterogeneous surfaces on the behavior of moving water droplets at the nano-scale was verified. The behavior of the water droplets can be classified by their shapes into three groups. These groups can be seen in Figure 5. The water droplets in the first group move like a stream in that the droplet is attached to the surface and stretches continuously. An example of the first group is $E_3H_2F_1$ shown in Fig. 5 (a). In this case, the water molecules above the pillar tops moved in the direction the force was applied while the pillars restricted the movement of the molecules below the pillar tops. Consequently the water droplet continued to stretch and finally merged into a stream because the size of the droplet outgrew the domain which had periodic boundaries. The second group seen in Fig. 5 (b) is characterized by a tear-drop or an elongated hemispherical shape due to the distorted water droplet. Similarly to the first group, the water molecules move and they are restricted by the pillar. However, the water droplet did not

stretch continuously in this group. And it maintained its distorted shape over time. The last group consists of the water droplets that maintain their initial spherical shape during their movement. Most of the static cases in the Cassie-Baxter state were in this group. The pillars do not greatly affect the water droplet because nearly all of water molecules are above the pillar tops. This group seen in Fig. 5 (c) is the most hydrophobic among the groups.

In order to evaluate the dynamic state of the water droplet quantitatively, the advancing and receding angles of the moving water droplets were used. The method to get the advancing and receding contact angles is similar to that used by *Hong et al* [28]. The difference in the advancing and receding contact angles is more important than their individual values. Furthermore many studies also use the difference in the cosines of the receding and advancing contact angles which is related to dynamic hydrophobicity of the surface [30-32]. A large difference in the cosines of the receding and advancing contact

angles shows a hydrophilic surface and a low value shows a hydrophobic surface [27-29, 33].

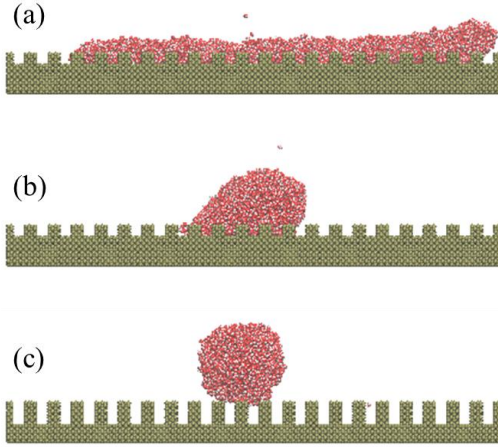


Figure 5 Examples of the three groups of the water droplet shape; (a) $E_3H_2F_2$ (b) $E_2H_2F_1$ (c) $E_4H_4F_3$

The results of the dynamic water droplets show some oscillation of the contact angles because the water droplets move and changes shapes continuously. The fitting equation Eq. (4) was applied to clarify the change of the contact angle over time.

$$\theta_{\text{Ad or Re}} = \exp(A \cdot \ln t + B) \quad (4)$$

where Ad or Re means the advancing or receding angle respectively. A and B are constants for each case, and t is the time the force was applied. This equation gives quantitative values for the advancing and receding contact angles at 5ns as used by Jeong *et al* [28]. and Ambrosia *et al* [29]. Figure 6 shows the examples of plots of the advancing and receding contact angles and fitting function line for 5ns.

In this way, the water droplets which are classified by their shapes as mentioned above can be evaluated quantitatively. The advancing and receding contact angles of a moving water droplet representative of the first group can be seen in Fig. 6 (a). In this case, the contact angles exist for about 1ns because the water droplet merges into a stream after 1ns. As a result, the contact angles cannot be measured beyond about 1 ns for this case. However, by using the predicted contact angles at 5ns, the case is evaluated. The cases in this group have a large difference in the advancing and receding angles. The values of the differences between the advancing and receding contact angles are 80° or higher, and the $\cos \theta_{\text{Re}} - \cos \theta_{\text{Ad}}$ values are 1.25 or higher. Fig. 6 (b) shows the contact angles of the second group. The differences between the advancing and receding contact angles of the second group are smaller than those of the first group because of the larger receding contact angles. The cases in this group have a band of difference in values between 10° and 80° with $\cos \theta_{\text{Re}} - \cos \theta_{\text{Ad}}$ values between 0.125 and 1.25. At last, the contact angles in the third group are plotted in Fig. 6 (c). In this case, the advancing and receding contact

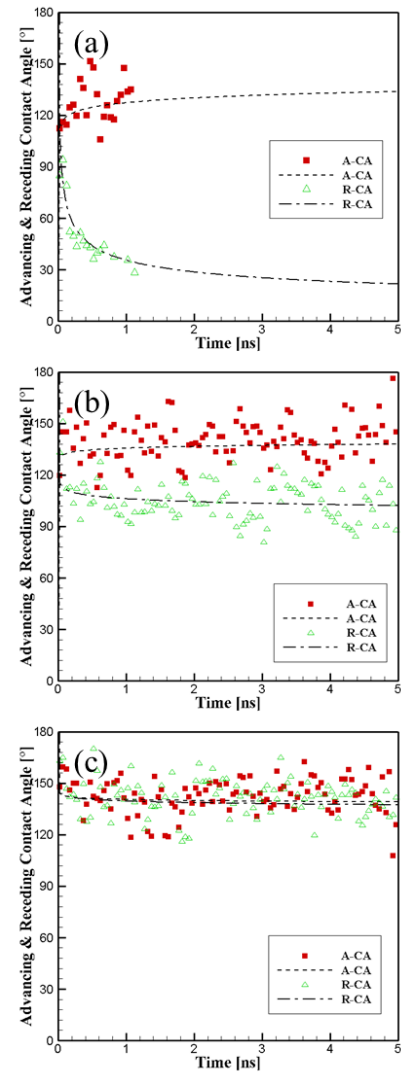


Figure 6 Examples of the fitting function line to evaluate the advancing and receding contact angle over 5ns; (a) $E_3H_2F_2$, (b) $E_1H_1F_2$, (c) $E_1H_4F_3$

angles are almost the same since the shape of the water droplets maintain their initial spherical shape. The differences in the angles for this group are under 10° with $\cos \theta_{\text{Re}} - \cos \theta_{\text{Ad}}$ values also small under 0.125. These small differences mean that these surfaces are dynamically hydrophobic.

The behavior of water droplets on homogeneous surfaces whose pillars and plates have the same characteristic energy were compared with previous studies. Figure 7 shows the differences in the cosines of the advancing and receding contact angles of the moving water droplets according to the dimensionless pillar height H . The results of the water droplets on the homogeneous surface can be seen in Fig. 7 (b). The $\cos \theta_{\text{Re}} - \cos \theta_{\text{Ad}}$ values have maximum values corresponding to the stream shape at H_1 or H_2 for each applied force. At H_3 which is higher than 10 \AA the $\cos \theta_{\text{Re}} - \cos \theta_{\text{Ad}}$ values decrease and the shape of the water droplet changes from stream to

distorted sphere or sphere. Then the $\cos \theta_{\text{Re}} - \cos \theta_{\text{Ad}}$ values generally maintain their respective values and shapes as the pillar height increases. This means that the surface with a higher pillar height is more dynamically hydrophobic than that with a lower pillar height. Furthermore, the $\cos \theta_{\text{Re}} - \cos \theta_{\text{Ad}}$ values increase as the applied force increases. For example, the $\cos \theta_{\text{Re}} - \cos \theta_{\text{Ad}}$ value increases from 0.21 to 0.78 to 1.90 at H_1 according to the magnitude of the applied force. This means that the surface is less hydrophobic as the applied force gets stronger. These results about the effects of the pillar height and the magnitude of the applied force corresponds with other previous studies by Jeong *et al* [28], and Ambrosia *et al* [29].

The heterogeneous surfaces investigated had pillars with a stronger or weaker characteristic energy than that of the homogeneous surface while keeping the characteristic energy of the plate constant. The characteristic energy of the plate was fixed at 0.3 kcal/mol. The weak pillar characteristic energy was 0.1 kcal/mol. The differences in the advancing and receding contact angles for this weak characteristic energy are seen in Fig. 7 (a). Similar to the homogeneous surface, the $\cos \theta_{\text{Re}} - \cos \theta_{\text{Ad}}$ values have a maximum value and then maintain a small value as the pillar height increases beyond a specific height. However, the $\cos \theta_{\text{Re}} - \cos \theta_{\text{Ad}}$ values in this case have the maximum value at H_1 and the values of $\cos \theta_{\text{Re}} - \cos \theta_{\text{Ad}}$ (0.08, 0.53 and 1.63) are smaller than that of homogeneous cases for their respective applied forces. The $\cos \theta_{\text{Re}} - \cos \theta_{\text{Ad}}$ values are almost the same at about 0.08 for all dimensionless pillar heights of H_2 or higher. The applied force affects the $\cos \theta_{\text{Re}} - \cos \theta_{\text{Ad}}$ value at H_1 but does not have much effect at higher pillar heights. Judging from the static state results, the cases in the Wenzel state are influenced by the magnitude of the applied force, but those in the Cassie-Baxter state are not because, in the Wenzel state, the water molecules under the pillar tops are moved by the applied force and restricted by the pillars. As the applied force increases the droplets for the droplets which were in the Wenzel state, the tension between the molecules on top of the pillars being pushed by the force and the molecules between the pillars being restricted by the pillars increases and causes the droplet to be stretched more. On the other hand, the water droplet in the Cassie-Baxter state is on the pillar tops so the pillars do not restrict the movement of the water droplet as the force is applied. As a result, the weak characteristic energy of the pillar makes the surface more hydrophobic compared with the homogeneous surface since the droplets were in the Cassie-Baxter state from H_2 instead of H_3 .

The cases with the stronger pillar characteristic energy of 0.5 kcal/mol show very interesting results compared with the others. The $\cos \theta_{\text{Re}} - \cos \theta_{\text{Ad}}$ values are seen in Fig. 7 (c). In these cases, the effect of the pillar height is different than the other cases which have the weaker pillar characteristic energy. When the strong force is applied, the $\cos \theta_{\text{Re}} - \cos \theta_{\text{Ad}}$ value

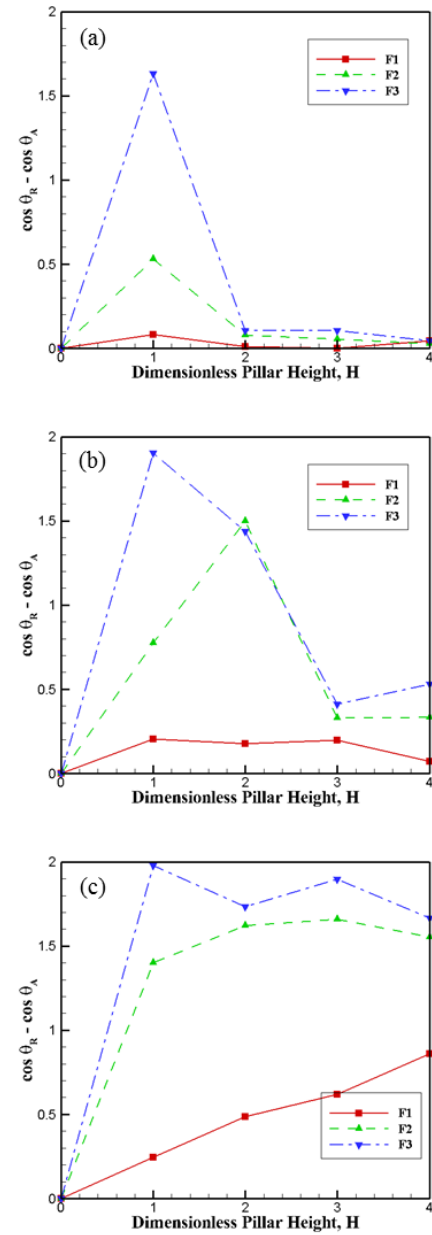


Figure 7 The differences in the cosines of the advancing and receding contact angles of the water droplets on the surface according to pillar height; (a) E_1 (b) E_2 (c) E_3

changes but the effect of the pillar height is very small. In the cases with the weak applied force, however, the $\cos \theta_{\text{Re}} - \cos \theta_{\text{Ad}}$ values increase as the height of the pillar increases. By using pillars which have a stronger characteristic energy, the surface becomes more hydrophilic contrary to other cases in which the pillars enhance the surface hydrophobicity beyond a certain pillar height.

Figure 8 shows the trend of $\cos \theta_{\text{Re}} - \cos \theta_{\text{Ad}}$ values as the characteristic energy of the pillar increases for each pillar height with different applied forces. In the cases of H_1 seen in

Fig. 8 (a), the applied force affects the $\cos \theta_{\text{Re}} - \cos \theta_{\text{Ad}}$ values to a great extent. For the F_1 case, the $\cos \theta_{\text{Re}} - \cos \theta_{\text{Ad}}$ values cannot reach the hydrophilic band while those of the F_3 cases are located in the hydrophilic band for each pillar characteristic energy. Only the strong pillar characteristic energy of F_2 was in the hydrophilic zone. However, for the H_2 , H_3 and H_4 cases seen in Fig. 8 (b), (c) and (d), respectively, show similar $\cos \theta_{\text{Re}} - \cos \theta_{\text{Ad}}$ values for the stronger applied forces. This means that the magnitude of the applied force affects the hydrophobicity more at the low pillar heights. On the other hand, the $\cos \theta_{\text{Re}} - \cos \theta_{\text{Ad}}$ values do not change much according to the pillar characteristic energy for the H_1 cases. However, for the H_2 , H_3 and H_4 cases, the $\cos \theta_{\text{Re}} - \cos \theta_{\text{Ad}}$ values have a large change according to the pillar characteristic energy. In detail, it shows that $\cos \theta_{\text{Re}} - \cos \theta_{\text{Ad}}$ increases rapidly between the pillar characteristic energy of 0.1 and 0.3 kcal/mol for the H_2 cases. And for the H_3 and H_4 cases, the $\cos \theta_{\text{Re}} - \cos \theta_{\text{Ad}}$ values increase rapidly between the pillar characteristic energy of 0.3 and 0.5 kcal/mol. This result indicates that the effect of the pillar characteristic energy is large at the higher pillar heights. And the pillar characteristic energy which is larger than that of the plate has a larger effect than the small pillar surface energy. As a result, as the pillar height increases, the effect of the applied force decreases and that of the pillar characteristic energy increases especially as the pillar characteristic energy increases from the homogeneous case.

CONCLUSIONS

This study investigated the behavior of a water droplet on the heterogeneous surfaces using MD simulations. We considered the effect of the magnitude of the applied force, the pillar height and the pillar characteristic energy. The simulations were carried out in two steps. At first, the static equilibrium state of the water droplet on each surface was obtained and evaluated. Then constant body forces were applied to the water droplets in the static equilibrium state. The water droplet showed various behaviors such as moving and changing shape. The behaviors were evaluated quantitatively using the contact angle hysteresis ($\cos \theta_{\text{Re}} - \cos \theta_{\text{Ad}}$).

The static state of the water droplets were either in the Wenzel or Cassie-Baxter state, depending on the pillar height and the pillar characteristic energy. When the pillar height is low, the water droplet is in the Wenzel state. As the pillar height increases, the surface becomes more hydrophobic and the state changes to the Cassie-Baxter state. For the change of the pillar characteristic energy, the large pillar characteristic energy makes the surface more hydrophilic. Therefore the water droplet at the same pillar height can be in the different states depending on the pillar characteristic energy.

The dynamic state of the water droplet can be classified into three groups by its shapes which depend on the pillar height, the pillar characteristic energy, and the magnitude of the

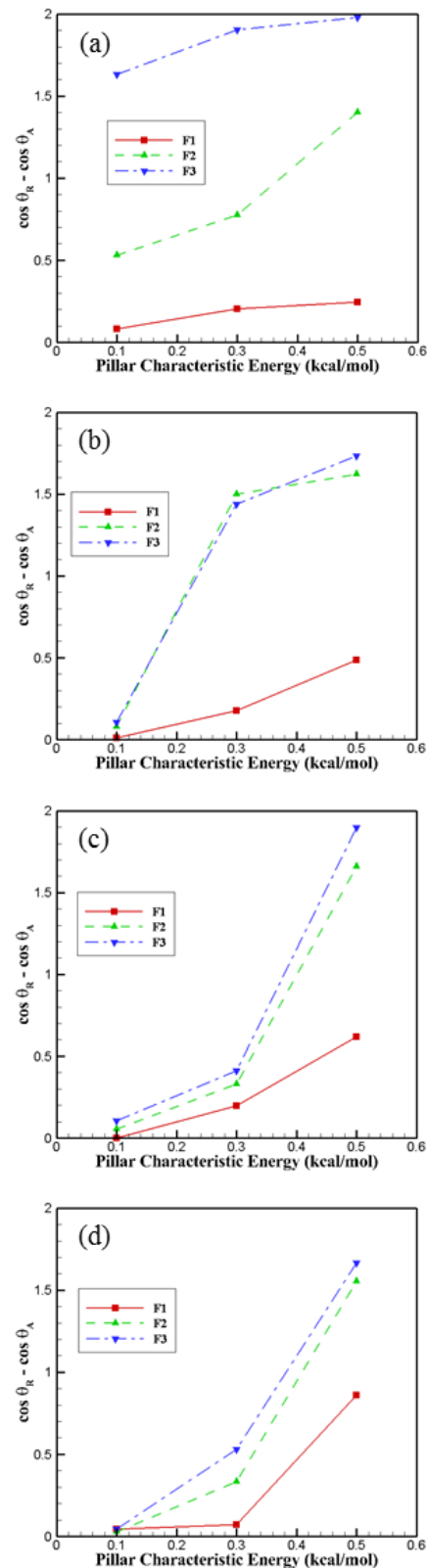


Figure 8 The differences in the cosines of the advancing and receding contact angles of the water droplets on the surface according to pillar characteristic energy; (a) H_1 (b) H_2 (c) H_3 (d) H_4

applied force. In the first group, the water droplet stretched and merged into a stream because of the different velocities of the advancing and receding parts. This occurs when a strong force is applied or the pillar characteristic energy is large with the droplet in the Wenzel state. The shape of the water droplet in the second group is a distorted sphere changed from the initial sphere when a weak force is applied to the droplet in the Wenzel state or when a strong force is applied to the droplet in the Cassie-Baxter state. The water droplet in the last group maintains its original spherical shape. This occurs only when the static droplet is in the Cassie-Baxter state.

The behavior of water droplet is also evaluated by using the difference in the cosines of the advancing and receding contact angles. This value can show the behavior of the water droplet quantitatively. The first group has the largest value, higher than 1.25, compared with other groups. The values in the third group is lower than 0.125 and those in the second group were in the range of 0.125 to 1.25. The effect of the variables on the hydrophobicity of the surface can be also evaluated by using the difference in the cosines of the advancing and receding contact angles. A large difference in the cosines of the receding and advancing contact angles shows a hydrophilic surface and a low value shows a hydrophobic surface.

In conclusion, the variables, the pillar height, the magnitude of the applied force and the pillar characteristic energy, affect the hydrophobicity of the surface. At first, as the pillar height increases, the hydrophobicity of the surface increases. This means that the hydrophobicity of the surface can be raised by increasing of the pillar height. Next, the stronger applied force makes the surface more hydrophilic because the force causes more tension between the molecules above the pillar tops and the molecules between the pillars. At last, the pillar characteristic energy also has a considerable effect on the hydrophobicity of the surface. The surface is more hydrophobic as the pillar characteristic energy decreases. The weak pillar characteristic energy especially has a large effect on the hydrophobicity of the surface at the low pillar heights. On the contrary to this, the strong pillar characteristic energy has a great effect on the hydrophobicity of the surface at the high pillar heights.

REFERENCES

[1] R. N. Wenzel, Resistance of solid surfaces to wetting by water. *Ind. Eng. Chem.* 28 (1936) 988-994

[2] A. B. D. Cassie, S. Baxter, Wettability of porous surfaces. *Trans. Faraday Soc.* 40 (1944) 546-551

[3] A. Marmur, Wetting on Hydrophobic Rough Surfaces: To Be Heterogeneous or Not To Be? *Langmuir.* 19 (2003) 8343-8348

[4] A.J.B. Milne, A. Amirfazli, The Cassie equation: How it is meant to be used. *Advances in Colloid and Interface Science.* 170 (2012) 48-55

[5] C.G.L. Furnidge, The sliding of liquid drops on solid surfaces and a theory for spray retention, *J. Colloid Sci.* 17 (1962) 309-324

[6] D. Öner, T.J. McCarthy, Ultrahydrophobic Surfaces. Effects of Topography Length Scales on Wettability, *Langmuir.* 16, (2000) 7777-7782

[7] Z. Yoshimitsu, A. Nakajima, T. Watanabe, K. Hashimoto, Effects of Surface Structure on the Hydrophobicity and Sliding Behavior of Water Droplets, *Langmuir.* 18 (2002) 5818-5822

[8] B. Krasovitski, A. Marmur, Drops Down the Hill: Theoretical Study of Limiting Contact Angles and the Hysteresis Range on a Tilted Plate, *Langmuir.* 21 (2005) 3881-3885

[9] A. I. ElSherbini, A. M. OJacobi, Retention forces and contact angles for critical liquid drops on non-horizontal surfaces, *J. Colloid Interface Sci.* 299 (2006) 841-849

[10] E. Pierce, F. J. Carmona, A. Amirfazli, Understanding of sliding and contact angle results in tilted plate experiments, *Colloids Surf. A.* 323 (2008) 73.

[11] L. Gao, T.J. McCarthy, Contact Angle Hysteresis Explained, *Langmuir.* 22 (2006) 6234-6237

[12] N. Yoshida, Y. Abe, H. Shigeta, A. Nakajima, H. Ohsaki, K. Hashimoto, T. Watanabe, Sliding Behavior of Water Droplets on Flat Polymer Surface, *J. Am. Chem. Soc.* 128 (2006) 743-747.

[13] A. Nakajima, Design of a Transparent Hydrophobic Coating, *J. Ceram. Soc. Jpn.* 112 (2004) 533-540

[14] M. Miwa, A. Nakajima, A. Fujishima, K. Hashimoto, T. Watanabe, Effects of the Surface Roughness on Sliding Angles of Water Droplets on Superhydrophobic Surfaces, *Langmuir.* 16 (2000) 5754-5760

[15] C. Lv, C. Yang, P. Hao, F. He, Q. Zheng, Sliding of Water Droplets on Microstructured Hydrophobic Surfaces, *Langmuir.* 26 (2010) 8704-8708

[16] M. Sakai, J. H. Song, N. Yoshida, S. Suzuki, Y. Kameshima, A. Nakajima, Direct Observation of Internal Fluidity in a Water Droplet during Sliding on Hydrophobic Surfaces, *Langmuir.* 22 (2006) 4906-4909

[17] P. Aussillous, D. Quéré, Liquid marbles, *Nature.* 411 (2001) 924-927

[18] S. Gogte, P. Vorobieff, R. Truesdell, A. Mammoli, F. van Swol, P. Shah, C. J. Brinker, Effective slip on textured superhydrophobic surfaces, *Phys. Fluids.* 17 (2005) 051701

[19] E. Bormashenko, B. Bormashenko, R. Oleg, On the Nature of the Friction between Nonstick Droplets and Solid Substrates, *Langmuir.* 26 (2010) 12479-12482

[20] L. Madadevan, Y. Pomeau, Rolling droplets, *Phys. Fluids.* 11 (1999) 2449-2453

[21] G. McHale, N. J. Shirtcliffe, M. I. Newton, Contact-Angle Hysteresis on Super-Hydrophobic Surfaces, *Langmuir.* 20 (2004) 10146-10149

[22] J. T. Hirvi, T. A. Pakkanee, Molecular dynamics simulations of water droplets on polymer surfaces, *J. Chem. Phys.* 125 (2006) 144712

[23] J. T. Hirvi, T. A. Pakkanee, Enhanced Hydrophobicity of Rough Polymer Surfaces, *J. Phys. Chem. B.* 111 (2007) 3336-3341

[24] J. T. Hirvi, T. A. Pakkanee, Wetting of Nanogrooved Polymer Surfaces, *Langmuir.* 23 (2007) 7724-7729

[25] J. T. Hirvi, T. A. Pakkanee, Nanodroplet impact and sliding on structured polymer surfaces, *Surf. Sci.* 602 (2008) 1810-1818

[26] J. C. Phillips, R. Braun, W. Wang, J. Gumbart, E. Taj-khorshid, E. Villa, C. Chipot, R.D. Skeel, L. Kale, K. Schul-ten, Scalable molecular dynamics with NAMD, *J. Comput. Chem.* 26 (2005) 1781-1802

[27] S. D. Hong, M. Y. Ha, S. Balachandar, Static and dynamic contact angles of water droplet on a solid surface using molecular dynamics simulation, *J. Colloid Interface Sci.* 339 (2009) 187-195

[28] W. J. Jeong, M. Y. Ha, H. S. Yoon, M. Ambrosia., Dynamic Behavior of Water Droplets on Solid Surfaces with Pillar-Type Nanostructures, *Langmuir.* 28 (2012) 5360-5371

[29] M. Ambrosia, M. Y. Ha, S. Balachandar, S. Dynamic Hydrophobicity on Flat and Pillared Graphite Surfaces with Different Pillar Surface Fractions, *J. Mechanical Science and Technology.* (2014) in press

- [30] S. Suzuki, A. Nakajima, Y. Kameshima, K. Okada, Elongation and contraction of water droplet during sliding on the silicon surface treated by fluoroalkylsilane, *Surface Science*. 557 (2004) 163-168
- [31] S. Suzuki, A. Nakajima, K. Tanaka, M. Sakai, A. Hashimoto, N. Yoshida, Y. Kameshima, K. Okada, Sliding behavior of water droplets on line-patterned hydrophobic surfaces, *Applied Surface Science*. 254 (2008) 1797-1805.
- [32] N. Yoshida, Y. Abe, H. Shigeta, A. Nakajima, H. Ohsaki, K. Hashimoto, T. Watanabe, Sliding Behavior of Water Droplets on Flat Polymer Surface, *J. Am. Chem. Soc.* 128 (2006) 743-747.
- [33] A. Carre, M.E.R. Shanahan, Drop Motion on an Inclined Plane and Evaluation of Hydrophobia Treatments to Glass, *J. Adhes.* 49 (1995) 177-185